MATERIALS SCIENCE

Slowing down of dynamics and orientational order preceding crystallization in hard-sphere systems

Felix Lehmkühler[1,2]*, Birgit Hankiewicz[3], Martin A. Schroer[4], Leonard Müller[1], Beatrice Ruta[5,6], Dina Sheyfer[1,2†], Michael Sprung[1], Kensuke Tono[7], Tetsuo Katayama[7,8], Makina Yabashi[7,8], Tetsuya Ishikawa[8], Christian Gutt[9], Gerhard Grübel[1,2]

Despite intensive studies in the past decades, the local structure of disordered matter remains widely unknown. We show the results of a coherent x-ray scattering study revealing higher-order correlations in dense colloidal hard-sphere systems in the vicinity of their crystallization and glass transition. With increasing volume fraction, we observe a strong increase in correlations at both medium-range and next-neighbor distances in the supercooled state, both invisible to conventional scattering techniques. Next-neighbor correlations are indicative of ordered precursor clusters preceding crystallization. Furthermore, the increase in such correlations is accompanied by a marked slowing down of the dynamics, proving experimentally a direct relation between orientational order and sample dynamics in a soft matter system. In contrast, correlations continuously increase for nonequilibrated, glassy samples, suggesting that orientational order is reached before the sample slows down to reach (quasi-)equilibrium.

INTRODUCTION

Structural higher-order correlations in liquids and glasses have been studied intensively in the past, mostly with computational methods (*1*). Hereby, the determination of orientational order parameters as defined by Steinhardt *et al.* (*2*) is a popular approach in simulation and microscopy studies on crystallization and vitrification (*3*–*6*). In this context, suspensions of colloidal hard spheres are a frequently investigated model system, particularly in pioneering studies on phase transitions (*3*, *5*, *7*–*15*). Depending on the volume fraction ϕ of the spherical particles, all accessible phases comprising the fluid, crystal, and glassy states can be prepared (*16*). Real-space imaging techniques such as confocal and stimulated emission depletion microscopy probe structural order locally; however, experimental limitations with respect to particle and system size, time scales, and composition remain (*14*). Here, x-ray scattering methods can provide complementary information. While standard scattering approaches allow accessing ensemble averaged information only, as expressed by the structure factor $S(q)$ as the Fourier transform of the radial pair-distribution function $g(r)$, the study of higher-order correlations by means of x-ray cross-correlation analysis (XCCA) based on coherent x-ray scattering is an elegant way to overcome the inherent averaging of conventional x-ray scattering.

Despite intensive research, the role of higher-order correlations in glasses and supercooled liquid remains an open question. This is, however, important to fully understand phase transitions and vitrification. Studies of higher-order correlations indicated the existence of a two-step crystallization process in colloidal suspensions (*4*, *17*–*19*). A recent simulation study on liquids has shown a nontrivial three-dimensional (3D) structure that has been identified by higher-order correlations (*20*). Furthermore, orientational order, such as an interplay of crystal-like and icosahedral order, appears to play a key role in the glass transition (*7*, *9*, *11*, *14*, *21*). XCCA can contribute to identify orientational order via higher-order correlations (*22*, *23*).

The use of higher-order intensity-correlation functions to obtain structural information beyond $S(q)$ has been first proposed by Kam in the 1970s (*24*) and is currently developed for structure determination of diluted solutions of nano- to microscopic particles such as biological virus particles (*25*). XCCA experiments can furthermore yield structural information from large ensembles of particles, as demonstrated by the observation of structural motifs in colloidal glasses (*26*). Recently, XCCA has been used in studies on the structure of soft matter and nanoscale systems, thin colloidal films, and crystals (*27*–*30*). XCCA revealed correlations of Bragg reflections from nanocrystals in solution and in 2D assemblies (*31*–*33*) as well as in in situ studies of colloidal self-assembly (*34*). Compared to microscopy, x-ray scattering allows studying particles on much smaller length scale—down to molecular and atomic levels. Furthermore, x-ray free-electron lasers (XFELs) can extend the accessible time range to femtoseconds, enabling x-ray scattering experiments to cover the whole time window between femtoseconds and several hours.

Here, we focus on the study of higher-order correlations in dense hard-sphere colloidal suspensions covering liquid, supercooled liquid, crystal, and glassy states. Combining coherent x-ray scattering from synchrotron and XFEL sources, we observe a strong increase in higher-order correlations over different length scales in the supercooled state. We can further relate the marked slowing

[1]Deutsches Elektronen-Synchrotron DESY, Notkestr. 85, 22607 Hamburg, Germany. [2]The Hamburg Centre for Ultrafast Imaging, Luruper Chaussee 149, 22761 Hamburg, Germany. [3]Institute of Physical Chemistry, Hamburg University, Grindelallee 117, 20146 Hamburg, Germany. [4]European Molecular Biology Laboratory (EMBL), Hamburg Outstation c/o DESY, Notkestr. 85, 22607 Hamburg, Germany. [5]Université de Lyon, Université Claude Bernard Lyon 1, CNRS, Institut Lumière Matière, 69622 Villeurbanne, France. [6]ESRF–The European Synchrotron, 38043 Grenoble cedex, France. [7]Japan Synchrotron Radiation Research Institute, 1-1-1 Kuoto, Sayo-cho, Sayo-gun, Hyogo 679-5198, Japan. [8]RIKEN SPring-8 Center, 1-1-1 Kuoto, Sayo-cho, Sayo-gun, Hyogo 679-5148, Japan. [9]Department of Physics, University of Siegen, Walter-Flex-Str. 3, 57072 Siegen, Germany.
*Corresponding author. Email: felix.lehmkuehler@desy.de
†Present address: Materials Science Division, Argonne National Laboratory, Argonne, IL 60439, USA.

down of the dynamics while approaching the glass transition to growing orientational order.

RESULTS

We measured coherent x-ray scattering patterns from poly(methyl methacrylate) (PMMA) hard-sphere systems suspended in decalin at beamlines ID10 at European Synchrotron Radiation Facility (ESRF), P10 at PETRA III, and the free-electron laser SPring-8-Angstrom Compact Free-Electron Laser (SACLA). A schematic drawing of the experimental setup is shown in Fig. 1. A phase diagram of hard-sphere systems is given in Fig. 2A. The particles studied here have a radius of r = 125.5 nm with a dispersity of $\Delta r/r$ = 0.07, and samples with volume fractions ranging from 0.49 to 0.58 have been prepared; the volume fractions studied are marked by crosses in the phase diagram in Fig. 2A. Studied volume fractions cover fluid, fluid-solid (FS) coexistence, and crystal and glassy states. To prove the reproducibility of the sample preparation (see Materials and Methods), we prepared selected volume fractions twice as shown here for ϕ = 0.577. For a dispersity of 0.07, crystallization may occur in the FS coexistence phase at volume fractions above 0.52 (*35*, *36*), while at higher volume fractions, a glassy state can be formed, typically for volume fractions above 0.55 (dark gray area in Fig. 2A). All volume fractions were prepared from the same randomly close-packed glassy state to avoid systematic errors for volume fraction determination (see Materials and Methods) (*37*). The sample was studied in addition at a volume fraction of 0.3 in the liquid state. To access structural snapshots of these fast-relaxing samples, we studied them using short x-ray pulses from the XFEL facility of SACLA (*38*).

Static structure and dynamics

For volume fractions $\phi > 0.49$, the samples have been characterized by measuring the static structure factors $S(q)$ (Fig. 2B) and the intermediate scattering function $f(q, t)$ using x-ray photon correlation spectroscopy (XPCS; see the Supplementary Materials). During the whole experimental time, we did not detect any Bragg reflections, indicating the absence of large crystallites in the illuminated volume. The position q_{nn} of the first maximum of $S(q)$, which corresponds to the typical next-neighbor distance, shifts toward larger q with increasing ϕ. This reflects the increasing packing density with higher volume fractions. The volume fractions were obtained by modeling q_{nn} with the Percus-Yevick model (*39*). The maximum value of $S(q)$, which is a measure for the magnitude of density-density correlations, varies only very weakly with ϕ. This deviation from the Percus-Yevick model, where the peak height increases monotonically as a function of ϕ, has been observed in previous x-ray scattering studies on PMMA-based hard-sphere colloids of similar size (*26*, *40*).

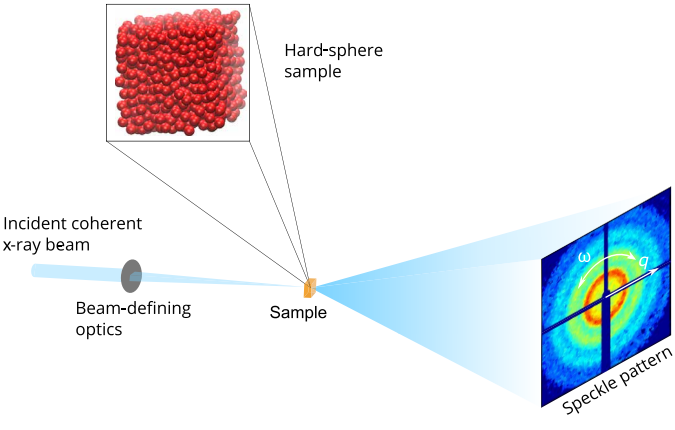

Fig. 1. Schematics of the experiment. The x-ray beam originating from the undulator source passes the optics (lenses and slits) that define a 10×10 – μm^2 coherent x-ray beam. It is scattered by the sample resulting in a so-called speckle pattern that is measured by a 2D detector at 5-m distance. The wave vector transfer q and the azimuth angle ω are indicated in the speckle pattern.

The relaxation times obtained from the intermediate scattering functions averaged over the first maximum of $S(q)$ as a function of the volume fraction ϕ are shown in Fig. 2C (see Materials and Methods and the Supplementary Materials for details). Typically, the relaxation time τ of hard-sphere systems increases with volume fraction while approaching dense-packed states (*7*–*9*, *41*), which is experimentally observed for $\phi \leq 0.545$ (region I). This behavior can be described by a Vogel-Fulcher-Tammann (VFT) law (*7*, *14*, *21*)

$$\tau(\phi) = \tau_0 \exp\left(\frac{D\phi_{VFT}}{\phi_{VFT} - \phi}\right) \quad (1)$$

with the so-called fragility index D, a VFT volume fraction ϕ_{VFT}, and a scaling time τ_0. We find D = 0.35, which is in good agreement with previous studies (*7*), and ϕ_{VFT} = 0.56. The latter appears to be slightly smaller than in other studies; however, we attribute this to the influence of dispersity and the systematic error in estimating ϕ (see Materials and Methods).

For $\phi \geq 0.545$ (region II), the relaxation times stay constant around 400 s. While this behavior has been reported for soft particles (*42*), equilibrated hard-sphere glasses typically show a continuous slowing down with increasing ϕ. Thus, we subdivide the samples in the following discussion into two regimes: The first, samples in region I, is in equilibrium and allows studying the fluid and fluid-crystalline state and the crystallization behavior of hard spheres. The samples in region II represent quenched glassy samples out of equilibrium.

Higher-order correlations

Higher-order correlations are quantified by the correlation function $\Psi_\ell(q)$ as the variance of the Fourier coefficients of order ℓ with respect to the azimuth angle ω (see Materials and Methods for details) (*43*). We plot $\Psi_\ell(q)$ for four selected volume fractions as a function of wave vector transfer q and Fourier component ℓ (Fig. 3), comprising a low volume fraction of ϕ = 0.522 (region I), a sample with higher volume fraction of ϕ = 0.577 (region II), a crystalline (face-centered cubic) sample (*31*), and the diluted sample at ϕ = 0.30. Above each $\Psi_\ell(q)$ map, the average $\langle\Psi_\ell(q)\rangle_\ell$ over all ℓ values is presented. For the noncrystalline samples, Ψ_ℓ is found to be weak, in the order of 10^{-4}, which is about two orders of magnitude below the results for the crystalline sample. This underlines the need of a sufficient statistical accuracy, in this case by measuring more than 10^3 to 10^4 diffraction patterns from independent sample spots.

Experiments and simulation of (quasi-)2D model structures (*30*, *43*, *44*) demonstrated that maxima of $\Psi_\ell(q)$ reflect the dominance of a certain local orientational order. Here, $\Psi_\ell(q)$ does not vary significantly with ℓ at a fixed q for the noncrystallized samples. Instead, we observe a very smooth distribution of Fourier coefficients for a fixed q value for both even and odd coefficients. The break of the Friedel symmetry, i.e., $I(q_x, q_y) \neq I(-q_x, -q_y)$ in our case, leads to the appearance of odd symmetries and can smear out

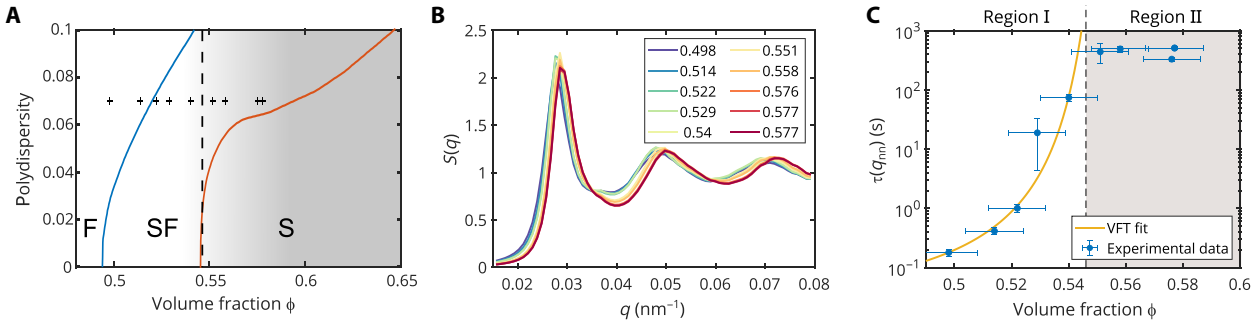

Fig. 2. Static structure and dynamics of the hard-sphere suspensions. (**A**) Calculated phase diagram of hard spheres with a triangular size distribution [adapted from (*35*)]. The solid lines reflect the coexistence lines between fluid (F), fluid-crystal coexistence (SF), and solid states (S) where the glassy state or multiple crystalline states can be found. The dashed line marks the transition from regions I to II shown in subpanel (C). The gray area marks the region where the glassy states were observed. The black crosses mark the volume fractions studied in this work. (**B**) Static structure factor $S(q)$. The legend indicates the corresponding volume fractions ϕ. (**C**) Relaxation times τ obtained from XPCS measurements as a function of volume fraction ϕ at q_{nn}. The orange line represents a fit to the Vogel-Fulcher-Tammann (VFT) law (Eq. 1) with $\phi_G = 0.56$. The black dashed line separates the liquid, equilibrated samples (region I), and the quenched glassy samples (region II). The relaxation time for diffusing particles is $\tau_{diffusion}(q_{nn}) = 2.3$ ms (see the Supplementary Materials).

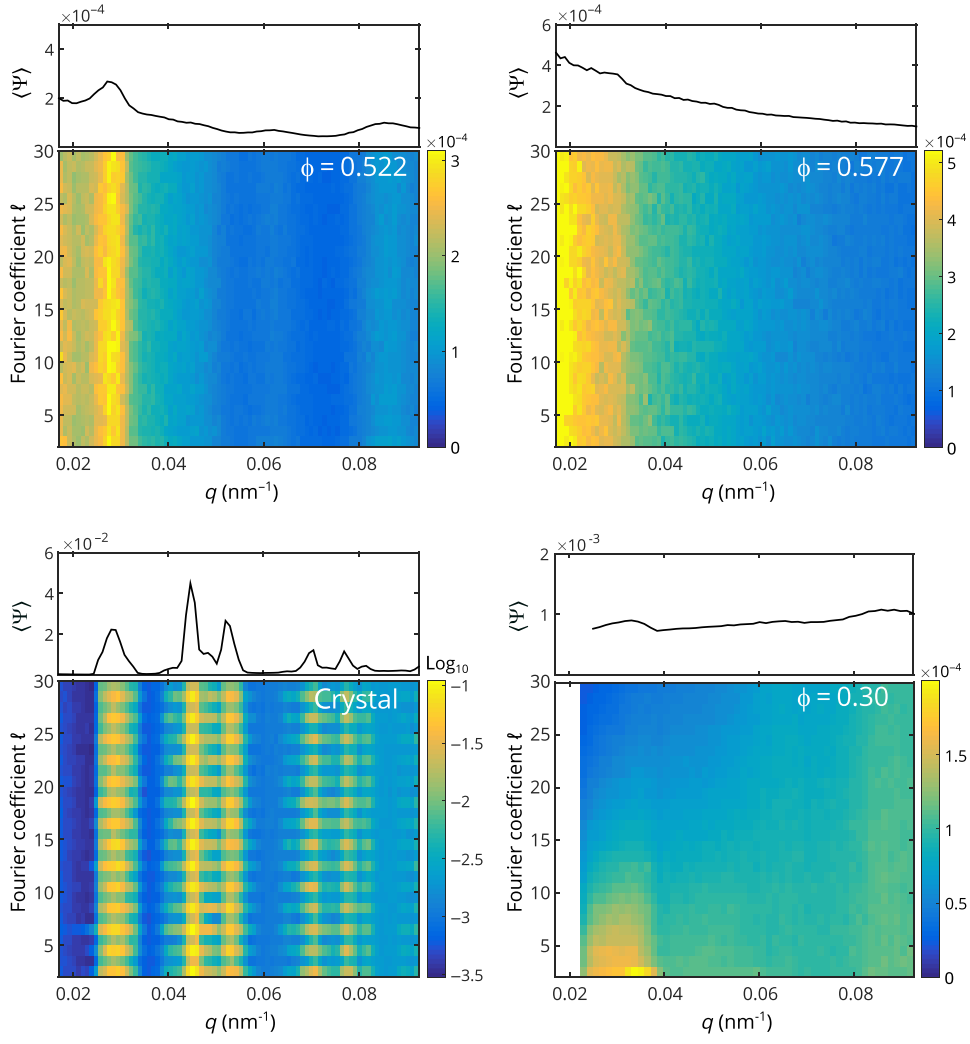

Fig. 3. Orientational-order patterns $\Psi_\ell(q)$. Three different volume fractions ($\phi = 0.522$, FS coexistence state; $\phi = 0.577$, glassy state; $\phi = 0.3$, fluid state) and a crystal state at $\phi = 0.52$ are shown. On top of each pattern, the average $\langle\Psi_\ell(q)\rangle_\ell$ is shown. For $\phi = 0.3$, q values smaller than 0.022 nm^{-1} could not be accessed. Note the different color scales for the individual patterns.

the even coefficients (*43*). This can be associated with experimental limitations when dealing with 3D samples, i.e., a nonflat Ewald sphere (*44*, *45*) and the contribution of Fresnel diffraction in coherent diffraction from samples with nonzero thickness (*46*). The crystalline sample did show incomplete Debye-Scherrer rings so that the symmetry is preserved at the Bragg reflections. The correlation functions differ weakly with (even) ℓ at fixed q, which is connected to the shape and width of the Bragg reflections (*31*, *44*). At q values where no Bragg peaks are observed, no notable higher-order correlations can be measured.

For the noncrystalline samples, a particular q dependence of $\Psi_\ell(q)$ is found for all ℓ. The dilute sample at $\phi = 0.30$ shows a weak peak at small ℓ around q_{nn}. For $\phi = 0.522$, a prominent maximum is found near q_{nn}, i.e., the peak position of the corresponding 2-point structure factor $S(q)$. For $\phi = 0.577$, one observes a monotonic decrease in $\Psi_\ell(q)$ as a function of q without pronounced maximum. As no particular Fourier component dominates for these samples, we choose the average $\langle\Psi_\ell(q)\rangle_\ell$ with respect to ℓ as a measure of the strength of higher-order correlations, as exemplary shown on top of Fig. 3 and for all volume fractions studied in Fig. 4A.

In general, we observe that $\langle\Psi_\ell(q)\rangle_\ell$ grows with increasing volume fraction ϕ, most prominently at small q. We stress that the correlation functions $\langle\Psi_\ell(q)\rangle_\ell$ of the two independently prepared samples at $\phi = 0.577$ differ by less than 4×10^{-6} corresponding to less than 2%, proving the reproducibility of the measurements. Because of the normalization to the mean intensity, the results are not affected by form-factor residues. For $\phi > 0.49$, $\langle\Psi_\ell(q)\rangle_\ell$ decreases with increasing q. We model the behavior at small q empirically with a power law $\langle\Psi_\ell(q)\rangle = a \times q^{-b}$ for the q range below 0.02 nm^{-1} and between 0.034 and 0.047 nm^{-1}, as shown in Fig. 4A for $\phi = 0.498$ by the black dashed line. The slope is given by the exponent b shown in the inset in Fig. 4A. For the dilute sample at $\phi = 0.30$, only weak changes as a function of q can be found. We have to note that because of setup constraints, the accessible q range was limited to a minimum value of 0.025 nm^{-1} for this sample studied at SACLA. The higher overall amplitude around 10^{-3} can be connected to the higher degree of coherence at SACLA (*47*) compared to the storage-ring experiments and thus better defined speckles (*48*). Comparing the observations for all volume fractions, we find (i) an increase in higher-order correlations with increasing volume fraction and (ii) a decrease in correlations with increasing q.

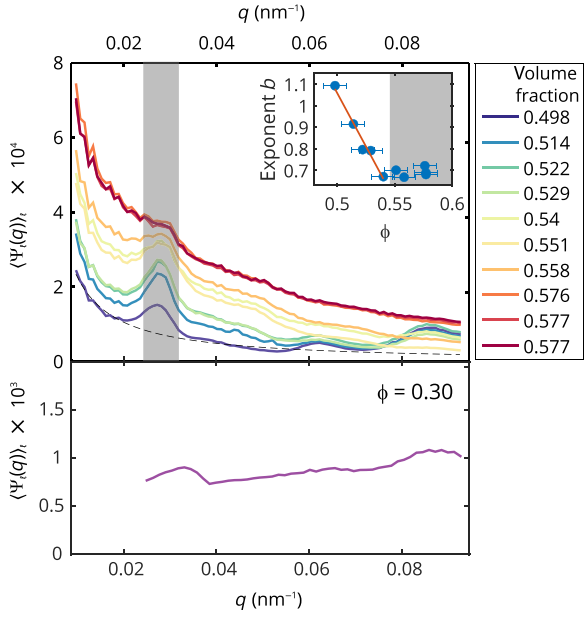

Fig. 4. Correlation function $\langle\Psi_\ell(q)\rangle_\ell$. Top: $\langle\Psi_\ell(q)\rangle_\ell$ for volume fractions above 0.49. The gray area marks the region around q_{nn}. The inset shows the fitted slope b from the power-law fit $\langle\Psi_\ell(q)\rangle = a \times q^{-b}$ of $\langle\Psi_\ell(q)\rangle_\ell$ at small q, and the black dashed line represents exemplary the fit for $\phi = 0.498$. **Bottom:** $\langle\Psi_\ell(q)\rangle_\ell$ for the fluid sample at $\phi = 0.3$.

Most intriguingly, we observe pronounced maxima around q_{nn} for all samples, indicating enhanced higher-order correlations within the next-neighbor shell. The shape and height of this first maximum depend strongly on the volume fraction with the lower volume fractions being more pronounced than the higher ones. The samples from region I ($\phi < 0.545$) also display maxima at larger q, which are basically absent for the samples in region II. The emergence of such higher-order correlations at distinct q values suggests the presence of ordered structures in the fluid and fluid-crystal coexistence phase, which are not detectable via the static structure factor $S(q)$. In the glassy state ($\phi > 0.55$), $\langle\Psi_\ell(q)\rangle$ is characterized by weaker q modulations, indicating the absence of preferred length scales, but increased contributions at low q values that will be discussed below. The correlations at q_{nn} suggest the appearance of a higher-ordered next-neighbor shell in the fluid-crystalline phase. The formation of crystalline precursor clusters is predicted in simulation studies on crystallization of hard-sphere systems, favoring a two-step crystallization mechanism via precursors (*3*, *4*, *17*, *18*, *49*). In those studies, an increase in higher-order correlations is interpreted as a precursor of crystallization. The decrease and disappearance of the correlation peak at q_{nn}, together with the global increase of $\langle\Psi_\ell(q)\rangle$ in region II, can be interpreted in the framework of LFS (locally favored structures) (*7*, *14*, *21*). The growth of such LFS has been reported for supercooled dispersions close to the glass transition. Consequently, correlations increase over longer length scales, resulting in an increase in $\langle\Psi_\ell(q)\rangle$ over a broad q range without a prominent contribution on a preferred length scale, e.g., at q_{nn}.

We want to quantify our observations by a more detailed inspection of the correlation functions. First, we focus on $\langle\Psi_\ell(q_{nn})\rangle_\ell$ and $S(q_{nn})$ as a function of volume fraction. The results are shown in Fig. 5A. The structure factor height changes only slightly with maximum changes of 11%. There is no connection to the volume fraction observable. $\langle\Psi_\ell(q_{nn})\rangle_\ell$ reflects the observations from Fig. 4. It increases linearly with ϕ, resulting in a total increase of a factor of 2.1 for the studied volume fractions. This overall behavior is reflected by a linear fit expressed by the solid line.

Second, the behavior at small q values is highlighted as well in Fig. 5A, showing $\langle\Psi_\ell(q_{mro})\rangle$ as a function of ϕ. The q value was chosen to correspond to a medium-range order on length scales of about 500 nm, yielding $q_{mro} \approx 0.4 \times q_{nn} = 0.012$ nm^{-1}. Similar to the results for q_{nn}, the data can be described best by a linear increase over the whole ϕ range by a factor of 3. These changes indicate the formation of substantial medium-range order in supercooled and glassy states, exceeding the observations at the next-neighbor distance.

Third, we connect the sample's dynamics and the correlation functions at q_{nn} and q_{mro}. In Fig. 5B, we recall $\tau(q_{nn})$ and compare it to $\tau(q_{mro})$ as a function of $\langle\Psi\rangle$ shown in Fig. 5A (the data are shown as a function of ϕ in fig. S4). Because of the de Gennes narrowing, the

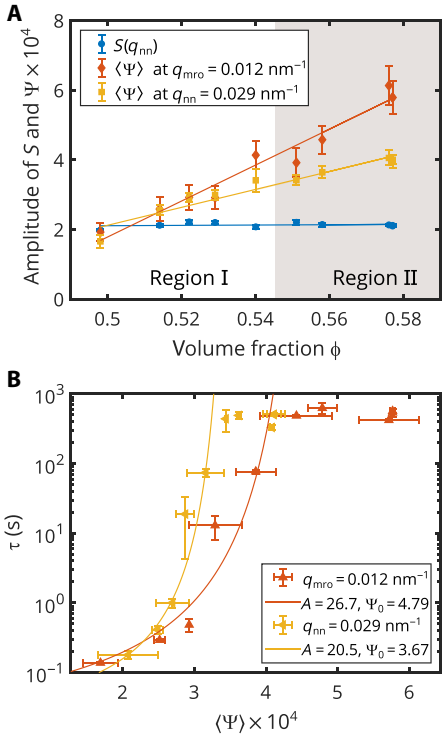

Fig. 5. Correlations and dynamics. (**A**) Amplitude of $S(q_{nn})$ and $\langle\Psi_\ell(q)\rangle_\ell$ at q_{mro} = 0.012 nm^{-1} and q_{nn} = 0.029 nm^{-1}. The lines are linear fits as guides to the eye. (**B**) Relaxation time τ at q_{mro} and q_{nn} as a function of $\langle\Psi\rangle$ shown in (A). The lines are fits to Eq. 2 for $\phi < \phi_G = 0.56$.

relaxation times are similar at both q values (see fig. S3). We find that the slowing down of the sample dynamics is accompanied by an increase in $\langle\Psi_\ell\rangle_\ell$ at both q_{nn} and q_{mro} in the fluid regime region I. Moreover, in region II where the relaxation times do not vary significantly with ϕ, the higher-order correlations continuously increase similarly to region I. In contrast to the static structure factor $S(q)$, the higher-order correlations accessed by $\Psi_\ell(q)$ provide more detailed information on sample structure, particularly reflecting correlations between dynamical and structural changes in the vicinity of crystallization and glass transition. With the VFT behavior of the relaxation time (Fig. 2) and the linear relation $\Psi \propto \phi$ shown in Fig. 5A, we obtain the relation

$$\tau \propto \exp\left(\frac{A\Psi_0}{\Psi_0 - \Psi}\right) \quad (2)$$

with constants A and $\Psi_0 = \Psi(\phi_G)$. Fits to this equation for samples from regime I are shown as well in Fig. 5B. This model agrees with the universal relation between structural order parameters and dynamics found recently by Tong and Tanaka (*21*) from simulations on supercooled liquids. We determine structure-dynamics relations over different length scales, particularly at the next-neighbor distance and at medium-range order. The relaxation time at q_{nn} increases at lower values of $\langle\Psi\rangle$ than at q_{mro}. This suggests the first formation of order at the next-neighbor distance leading to the slowing down, followed by emerging order at medium length scales.

DISCUSSION

We used angular x-ray intensity correlation functions to characterize the structure of liquid and glassy colloidal hard-sphere samples at volume fractions between 0.3 and 0.6. Distinct features can be observed that change with volume fraction. First, with increasing volume fraction, contributions at low q increase. This can be interpreted as growth of medium-range order, which is largely unexplored by conventional scattering techniques. We found an exponential relation $\langle\Psi_\ell(q)\rangle_\ell \propto q^{-b}$, where b is a slowly decreasing function of ϕ for $\phi < 0.545$ (region I) and $b \approx$ const. for amorphous samples in region II. In the fluid phase ($\phi = 0.3$), the medium-range contributions vanish.

Second, a maximum appears in the correlation functions in the vicinity of the structure-factor peak at lower volume fractions where the sample is in the fluid and fluid-crystal state. The increase in higher-order correlations suggests the occurrence of ordered structures under supercooled conditions in the liquid/crystalline coexistence phase. Furthermore, high-q peaks can be observed whose positions do not correspond to the position of the Bragg peaks in the crystal phase. This suggests ordering on different length scales preceding crystallization. The decrease in the maximum together with the increase in $\langle\Psi_\ell(q)\rangle$ may be a fingerprint of the growth of LFS, i.e., correlations increase over different length scales without a prominent contribution on the next-neighbor distance.

Third, we found a clear correlation between the increase in higher-order correlations and the slowing down of the sample over a wide q range. Dynamics slow down first at the next-neighbor distance, while a higher particle concentration and thus higher degree of local order are needed at the medium range. Our data could be modeled by a VFT-type relation proposed recently from simulations on different types of colloidal particles (*21*). Furthermore, higher-order correlations continuously increase for the out-of-equilibrium glassy samples, while the relaxation time does not change. This suggests that higher-order correlation increase before the dynamics slows down in the vicinity of the glass transition.

In contrast to the strong changes of the higher-order correlations over the studied volume fraction regime, variations of the static structure factor are very weak and mostly unsystematic. In conclusion, the XCCA method allows us to gain more details on structural properties and offers an increased sensitivity to structural changes compared to conventional scattering methods. Higher-order correlations as detected by XCCA allow tracking of structure formation in amorphous materials and in the vicinity of phase transitions in a superior way than by $S(q)$ only. Furthermore, we show that the XCCA approach provides experimental measures of local orientational order, verifying predictions from state-of-the-art simulation and theory. Our results are in agreement with simulation and microscopy studies, reporting growth of static and dynamic length scales at high particle concentrations (*7*, *10*, *14*, *21*, *50*). However, compared to microscopy studies, where the investigation is typically focused on the role of locally favored structures (*7*, *14*), correlation analysis of scattering data enables accessing structural information over different length scales as reported here. Moreover, with the advent of free-electron laser sources, such x-ray correlation studies are not limited in time and length scales and can be extended to liquid phases such as here for $\phi = 0.30$ and atomic resolutions, quantifying local structures for a broad range of materials.

MATERIALS AND METHODS

X-ray cross correlation analysis

In XCCA experiments, the correlation function

$$C(q,\Delta)=\frac{\langle I(q,\omega)\,I(q,\omega+\Delta)\rangle_\omega-\langle I(q,\omega)\rangle_\omega^2}{\langle I(q,\omega)\rangle_\omega^2} \quad (3)$$

is studied for annuli of constant wave vector transfer $q = \frac{4\pi}{\lambda}\sin(\theta/2)$ from 2D coherent scattering patterns (*26*, *44*), as shown in Fig. 1. Here, ω denotes the azimuth angle, λ is the wavelength, and θ is the scattering angle. It was shown (*22*, *23*) that C can be written as combination of three- and four-point correlations, thus being a measure of higher-order correlations. It further scales with $1/N_s$, where N_s is the number of scatterers in the probed volume. Local order is typically studied by Fourier modes $\widehat{C}_\ell$ of C with respect to Δ. These are related to the angular Fourier coefficients of $I(q, \omega)$ via the Wiener-Khinchin theorem to

$$\widehat{C}_\ell(q)\propto |I_\ell(q)|^2 \quad (4)$$

Here, $\hat{I}_\ell(q)$ is the ℓth angular Fourier coefficient

$$\hat{I}_\ell(q)=\int_0^{2\pi}\bar{I}(q,\omega)\,e^{il\omega}d\omega \quad (5)$$

of the normalized intensity ring $\bar{I}(q,\omega)=I(q,\omega)/\langle I(q,\omega)\rangle_\omega$, with the conventional scattering intensity $\langle I(q,\omega)\rangle_\omega$, extracted from a single diffraction pattern.

We introduced the ensemble average

$$\Psi_\ell(q)=\langle\hat{I}_\ell(q)^2\rangle_{N_p}-\langle\hat{I}_\ell(q)\rangle_{N_p}^2 \quad (6)$$

that allows tracking higher-order correlations in diffraction patterns (*43*), where $\langle\ldots\rangle_{Np}$ denotes the ensemble average over N_p patterns. In special cases, such as 2D samples, a maximum at a certain Fourier coefficient ℓ can directly be connected to the corresponding local order, e.g., hexagonal arrangements result in maxima for $l = 6$ and higher orders thereof (l = 12,18,24, …) (*43*).

Sample preparation

First, a parent solution of PMMA hard spheres suspended in decalin was centrifuged for several hours to achieve a random close-packed sample with a volume fraction of $\phi_{rcp} \approx 0.64$. The PMMA particles were synthesized following (*51*, *52*). The spheres had a radius of $r = 125.5$ nm at a dispersity of $\Delta r/r = 0.07$, which allows the sample to crystallize (*36*). To achieve volume fractions between 0.5 and 0.6, a calculated amount of decalin was added, and the sample was stirred afterward. We estimate the absolute error of ϕ to 0.01, which is in agreement with recent studies (*37*). The samples were filled in quartz capillaries with a diameter of 0.7 mm and 10-μm wall thickness and briefly centrifuged to yield quenched samples. Last, the capillaries were sealed before being placed into the sample chamber. As a reference sample, we also measured a suspension at $\phi \approx 0.52$ that was stored for several months to allow crystallites to grow.

Experimental details

The coherent x-ray scattering experiments on the concentrated samples were performed at the beamline ID10 at ESRF (Grenoble, France) and at the beamline P10 at PETRA III at Deutsches Elektronen-Synchrotron (DESY) (Hamburg, Germany). In both cases, the sample capillaries were placed in a designated sample cell that was evacuated afterward. An 8-keV (ID10) or 7.9-keV (P10) coherent x-ray beam with a size of $10 \times 10\ \mu m^2$ was used, respectively. The coherent flux was 9×10^9 photons per second at ID10 and 10^9 at P10. To extract the static structure factor $S(q)$ from the scattering patterns, the particle form factor was determined by measuring a diluted sample. At ID10, the scattering patterns were measured with a Maxipix 2 × 2 detector with a pixel size of $55 \times 55\ \mu m^2$, whereas a Princeton Instruments charge-coupled device (CCD) camera ($20 \times 20 - \mu m^2$ pixel size) was used at P10. Both detectors were placed approximately 5 m downstream of the sample, resulting in a maximum achievable wave vector transfer of $q_{lim} \approx 0.12\ nm^{-1}$. To determine the dynamics of the samples, first, an XPCS run was performed by taking 300 to 1000 scattering patterns from one spot of the sample with exposure times between 0.01 to 0.1 s per pattern. Depending on the estimated relaxation times, a delay time of 0 to 5 s between two measurements was set. Furthermore, radiation damage is reduced in this way. The sample's relaxation times are determined by fitting the intermediate scattering functions $|f(q,t)|$ extracted from the intensity-time correlation functions g_2 (see Supplementary Materials for details). A direction-dependent analysis of the g_2 functions proves that the dynamics were isotropic; in particular, we did not find any indication from sedimentation during the experimental time (see the Supplementary Materials). Afterward, the XCCA measurements were performed by taking scattering patterns at 900 to 1200 different spots on the sample to detect different structural realizations of the sample. To achieve decent statistics, 10 to 20 scattering patterns were taken at each sample spot. The data were lastly analyzed following the scheme shown in (*43*).

Because of the fast relaxation times of the diluted fluid samples in the sub-millisecond regime, speckle patterns with decent statistics cannot be obtained at storage-ring sources. Therefore, these samples were measured at the free-electron laser SACLA using short x-ray pulses of approximately 5-fs duration. The experiment was performed at SACLA's EH3 of beamline BL3 at a photon energy of 8 keV. The pulse energy was (300 ± 40) μJ with a bandwidth of 5×10^{-3} (*53*) at a repetition rate of 20 Hz. Using Kirkpatrick-Baez mirrors, the beam size was $1.8 \times 1.5\ \mu m^2$ ($h \times v$) at the sample position. The sample capillaries were placed into a holder that was mounted in the multiple-application X-ray imaging chamber (MAXIC) sample chamber of BL3 (*54*). To resolve the structure factor of the samples, the detector [dual multiport CCD (MPCCD) (*55*), i.e., two sensors with 1024 × 512 pixels each with individual pixel size of 50 μm × 50 μm] was placed at a distance of 3 m downstream of the sample. For both samples, at least 20,000 single-shot speckle patterns were taken for the XCCA at different spots on the capillary.

SUPPLEMENTARY MATERIALS

Supplementary material for this article is available at http://advances.sciencemag.org/cgi/content/full/6/43/eabc5916/DC1

REFERENCES AND NOTES

1. H. Tanaka, H. Tong, R. Shi, J. Russo, Revealing key structural features hidden in liquids and glasses. *Nat. Rev. Phys.* **1**, 333–348 (2019).
2. P. J. Steinhardt, D. R. Nelson, M. Ronchetti, Bond-orientational order in liquids and glasses. *Phys. Rev. B* **28**, 784–805 (1983).
3. E. Sanz, C. Valeriani, E. Zaccarelli, W. C. K. Poon, M. E. Cates, P. N. Pusey, Avalanches mediate crystallization in a hard-sphere glass. *Proc. Natl. Acad. Sci. U.S.A.* **111**, 75–80 (2014).
4. J. Russo, H. Tanaka, The microscopic pathway to crystallization in supercooled liquids. *Sci. Rep.* **2**, 505 (2012).
5. H. Tanaka, T. Kawasaki, H. Shintani, K. Watanabe, Critical-like behaviour of glass-forming liquids. *Nat. Mater.* **9**, 324–331 (2010).

6. U. Gasser, E. R. Weeks, A. Schofield, P. Pusey, D. Weitz, Real-space imaging of nucleation and growth in colloidal crystallization. *Science* **292**, 258–262 (2001).
7. M. Leocmach, H. Tanaka, Roles of icosahedral and crystal-like order in the hard spheres glass transition. *Nat. Commun.* **3**, 974 (2012).
8. W. Van Megen, P. Pusey, Dynamic light-scattering study of the glass transition in a colloidal suspension. *Phys. Rev. A* **43**, 5429–5441 (1991).
9. G. L. Hunter, E. R. Weeks, The physics of the colloidal glass transition. *Rep. Prog. Phys.* **75**, 066501 (2012).
10. A. J. Dunleavy, K. Wiesner, R. Yamamoto, C. P. Royall, Mutual information reveals multiple structural relaxation mechanisms in a model glass former. *Nat. Commun.* **6**, 6089 (2015).
11. C. Xia, J. Li, Y. Cao, B. Kou, X. Xiao, K. Fezzaa, T. Xiao, Y. Wang, The structural origin of the hard-sphere glass transition in granular packing. *Nat. Commun.* **6**, 8409 (2015).
12. S. Golde, T. Palberg, H. J. Schöpe, Correlation between dynamical and structural heterogeneities in colloidal hard-sphere suspensions. *Nat. Phys.* **12**, 712–717 (2016).
13. L. Berthier, D. Coslovich, A. Ninarello, M. Ozawa, Equilibrium sampling of hard spheres up to the jamming density and beyond. *Phys. Rev. Lett.* **116**, 238002 (2016).
14. J. E. Hallett, F. Turci, C. P. Royall, Local structure in deeply supercooled liquids exhibits growing lengthscales and dynamical correlations. *Nat. Commun.* **9**, 3272 (2018).
15. J. E. Hallett, F. Turci, C. P. Royall, The devil is in the details: Pentagonal bipyramids and dynamic arrest. *J. Stat. Mech.* **2020**, 014001 (2020).
16. P. N. Pusey, W. van Megen, Phase behaviour of concentrated suspensions of nearly hard colloidal spheres. *Nature* **320**, 340–342 (1986).
17. H. J. Schöpe, G. Bryant, W. van Megen, Two-step crystallization kinetics in colloidal hard-sphere systems. *Phys. Rev. Lett.* **96**, 175701 (2006).
18. P. Tan, N. Xu, L. Xu, Visualizing kinetic pathways of homogeneous nucleation in colloidal crystallization. *Nat. Phys.* **10**, 73–79 (2014).
19. J. Russo, H. Tanaka, Crystal nucleation as the ordering of multiple order parameters. *J. Chem. Phys.* **145**, 211801 (2016).
20. Z. Zhang, W. Kob, Revealing the three-dimensional structure of liquids using four-point correlation functions. *Proc. Natl. Acad. Sci. U.S.A.* **117**, 14032–14037 (2020).
21. H. Tong, H. Tanaka, Structural order as a genuine control parameter of dynamics in simple glass formers. *Nat. Commun.* **10**, 5596 (2019).
22. B. J. Ackerson, T. W. Taylor, N. A. Clark, Characterization of the local structure of fluids by apertured cross-correlation functions. *Phys. Rev. A* **31**, 3183–3193 (1985).
23. A. Denton, N. Ashcroft, High-order direct correlation functions of uniform classical liquids. *Phys. Rev. A* **39**, 426–429 (1989).
24. Z. Kam, Determination of macromolecular structure in solution by spatial correlation of scattering fluctuations. *Macromolecules* **10**, 927–934 (1977).
25. R. P. Kurta, J. J. Donatelli, C. H. Yoon, P. Berntsen, J. Bielecki, B. J. Daurer, H. De Mirci, P. Fromme, M. F. Hantke, F. R. N. C. Maia, A. Munke, C. Nettelblad, K. Pande, H. K. N. Reddy, J. A. Sellberg, R. G. Sierra, M. Svenda, G. van der Schot, I. A. Vartanyants, G. J. Williams, P. L. Xavier, A. Aquila, P. H. Zwart, A. P. Mancuso, Correlations in scattered x-ray laser pulses reveal nanoscale structural features of viruses. *Phys. Rev. Lett.* **119**, 158102 (2017).
26. P. Wochner, C. Gutt, T. Autenrieth, T. Demmer, V. Bugaev, A. D. Ortiz, A. Duri, F. Zontone, G. Grübel, H. Dosch, X-ray cross correlation analysis uncovers hidden local symmetries in disordered matter. *Proc. Natl. Acad. Sci. U.S.A.* **106**, 11511–11514 (2009).
27. M. A. Schroer, C. Gutt, F. Lehmkühler, B. Fischer, I. Steinke, F. Westermeier, M. Sprung, G. Grübel, Nano-beam x-ray microscopy of dried colloidal films. *Soft Matter* **11**, 5465–5472 (2015).
28. G. F. Mancini, T. Latychevskaia, F. Pennacchio, J. Reguera, F. Stellacci, F. Carbone, Order/disorder dynamics in a dodecanethiol-capped gold nanoparticles supracrystal by small-angle ultrafast electron diffraction. *Nano Lett.* **16**, 2705–2713 (2016).
29. A. C. Y. Liu, R. F. Tabor, M. D. de Jonge, S. T. Mudie, T. C. Petersen, Favored local structures in amorphous colloidal packings measured by microbeam x-ray diffraction. *Proc. Natl. Acad. Sci. U.S.A.* **114**, 10344–10349 (2017).
30. F. Lehmkühler, F. Schulz, M. A. Schroer, L. Frenzel, H. Lange, G. Grübel, Heterogeneous local order in self-assembled nanoparticle films revealed by x-ray cross-correlations. *IUCrJ* **5**, 354–360 (2018).
31. F. Lehmkühler, B. Fischer, L. Müller, B. Ruta, G. Grübel, Structure beyond pair correlations: X-ray cross-correlation from colloidal crystals. *J. Appl. Crystallogr.* **49**, 2046–2052 (2016).
32. D. Mendez, H. Watkins, S. Qiao, K. S. Raines, T. J. Lane, G. Schenk, G. Nelson, G. Subramanian, K. Tono, Y. Joti, M. Yabashi, D. Ratner, S. Doniach, Angular correlations of photons from solution diffraction at a free-electron laser encode molecular structure. *IUCrJ* **3**, 420–429 (2016).
33. N. Mukharamova, D. Lapkin, I. A. Zaluzhnyy, A. André, S. Lazarev, Y. Y. Kim, M. Sprung, R. P. Kurta, F. Schreiber, I. A. Vartanyants, M. Scheele, Revealing grain boundaries and defect formation in nanocrystal superlattices by nanodiffraction. *Small* **15**, 1904954 (2019).
34. I. Lokteva, M. Koof, M. Walther, G. Grübel, F. Lehmkühler, Monitoring nanocrystal self-assembly in real time using in situ small-angle x-ray scattering. *Small* **15**, 1900438 (2019).
35. M. Fasolo, P. Sollich, Equilibrium phase behavior of polydisperse hard spheres. *Phys. Rev. Lett.* **91**, 068301 (2003).
36. P. Sollich, N. B. Wilding, Crystalline phases of polydisperse spheres. *Phys. Rev. Lett.* **104**, 118302 (2010).
37. W. C. K. Poon, E. R. Weeks, C. P. Royall, On measuring colloidal volume fractions. *Soft Matter* **8**, 21–30 (2012).
38. M. Yabashi, H. Tanaka, T. Ishikawa, Overview of the SACLA facility. *J. Synchrotron Radiat.* **22**, 477–484 (2015).
39. M. S. Wertheim, Exact solution of the percus-yevick integral equation for hard spheres. *Phys. Rev. Lett.* **10**, 321–323 (1963).
40. E. D. Cola, A. Moussaïd, M. Sztucki, T. Narayanan, E. Zaccarelli, Correlation between structure and rheology of a model colloidal glass. *J. Chem. Phys.* **131**, 144903 (2009).
41. G. Brambilla, D. El Masri, M. Pierno, L. Berthier, L. Cipelletti, G. Petekidis, A. B. Schofield, Probing the equilibrium dynamics of colloidal hard spheres above the mode-coupling glass transition. *Phys. Rev. Lett.* **102**, 085703 (2009).
42. A.-M. Philippe, D. Truzzolillo, J. Galvan-Myoshi, P. Dieudonné-George, V. Trappe, L. Berthier, L. Cipelletti, Glass transition of soft colloids. *Phys. Rev. E* **97**, 040601 (2018).
43. F. Lehmkühler, G. Grübel, C. Gutt, Detecting orientational order in model systems by x-ray cross-correlation methods. *J. Appl. Crystallogr.* **47**, 1315–1323 (2014).
44. I. A. Zaluzhnyy, R. P. Kurta, M. Scheele, F. Schreiber, B. I. Ostrovskii, I. A. Vartanyants, Angular x-ray cross-correlation analysis (AXCCA): Basic concepts and recent applications to soft matter and nanomaterials. *Materials* **12**, 3464 (2019).
45. A. C. Y. Liu, R. F. Tabor, L. Bourgeois, M. D. de Jonge, S. T. Mudie, T. C. Petersen, Probing local order in glasses from limited-volume electron and x-ray diffraction. *J. Stat. Mech.* **2016**, 054046 (2016).
46. S. K. Sinha, M. Tolan, A. Gibaud, Effects of partial coherence on the scattering of x rays by matter. *Phys. Rev. B* **57**, 2740–2758 (1998).
47. F. Lehmkühler, C. Gutt, B. Fischer, M. A. Schroer, M. Sikorski, S. Song, W. Roseker, J. Glownia, M. Chollet, S. Nelson, K. Tono, T. Katayama, M. Yabashi, T. Ishikawa, A. Robert, G. Grübel, Single shot coherence properties of the free-electron laser SACLA in the hard x-ray regime. *Sci. Rep.* **4**, 5234 (2014).
48. T. Latychevskaia, G. F. Mancini, F. Carbone, The role of the coherence in the cross-correlation analysis of diffraction patterns from two-dimensional dense mono-disperse systems. *Sci. Rep.* **5**, 16573 (2015).
49. J. R. Savage, A. D. Dinsmore, Experimental evidence for two-step nucleation in colloidal crystallization. *Phys. Rev. Lett.* **102**, 198302 (2009).
50. T. Kawasaki, H. Tanaka, Structural signature of slow dynamics and dynamic heterogeneity in two-dimensional colloidal liquids: Glassy structural order. *J. Phys. Condens. Matter* **23**, 194121 (2011).
51. L. Antl, J. W. Goodwin, R. D. Hill, R. H. Ottewill, S. M. Owens, S. Papworth, J. A. Waters, The preparation of poly(methyl methacrylate) latices in non-aqueous media. *Colloid Surf.* **17**, 67–78 (1986).
52. C. Pathmamanoharan, C. Slob, H. N. W. Lekkerkerker, Preparation of polymethylmethacrylate latices in non-polar media. *Colloid Polym. Sci.* **267**, 448–450 (1989).
53. K. Tono, T. Togashi, Y. Inubushi, T. Sato, T. Katayama, K. Ogawa, H. Ohashi, H. Kimura, S. Takahashi, K. Takeshita, Beamline, experimental stations and photon beam diagnostics for the hard x-ray free electron laser of SACLA. *New J. Phys.* **15**, 083035 (2013).
54. C. Song, K. Tono, J. Park, T. Ebisu, S. Kim, H. Shimada, S. Kim, M. Gallagher-Jones, D. Nam, T. Sato, T. Togashi, K. Ogawa, Y. Joti, T. Kameshima, S. Ono, T. Hatsui, S. Iwata, M. Yabashi, T. Ishikawa, Multiple application x-ray imaging chamber for single-shot diffraction experiments with femtosecond x-ray laser pulses. *J. Appl. Crystallogr.* **47**, 188–197 (2014).
55. T. Kameshima, S. Ono, T. Kudo, K. Ozaki, Y. Kirihara, K. Kobayashi, Y. Inubushi, M. Yabashi, T. Horigome, A. Holland, K. Holland, D. Burt, H. Murao, T. Hatsui, Development of an x-ray pixel detector with multi-port charge-coupled device for x-ray free-electron laser experiments. *Rev. Sci. Instrum.* **85**, 033110 (2014).
56. G. Grübel, A. Madsen, A. Robert, *Soft Matter Characterization* (Springer Netherlands, 2008), pp. 953–995.
57. A. Madsen, A. Fluerasu, B. Ruta, *Synchrotron Light Sources and Free-Electron Lasers* (Springer International Publishing, 2018), pp. 1617–1641.
58. A. R. Sandy, Q. Zhang, L. B. Lurio, Hard x-ray photon correlation spectroscopy methods for materials studies. *Annu. Rev. Mater. Res.* **48**, 167–190 (2018).
59. M. Sikorski, Z. Jiang, M. Sprung, S. Narayanan, A. R. Sandy, B. Tieman, A graphical user interface for real-time analysis of XPCS using HPC. *Nucl. Instrum. Methods Phys. Res, Sect. A* **649**, 234–236 (2011).
60. L. Frenzel, F. Lehmkühler, I. Lokteva, S. Narayanan, M. Sprung, G. Grübel, Anomalous dynamics of concentrated silica-PNIPAm nanogels. *J. Phys. Chem. Lett.* **10**, 5231–5236 (2019).

Acknowledgments: We thank J. Russo, L. Janssen, and P. Wochner for discussion and proofreading and A. Schofield for the synthesis training of the hard-sphere particles. We acknowledge the European Synchrotron Radiation Facility for provision of synchrotron

radiation facilities, and we thank F. Zontone for assistance in using beamline ID10. Parts of this research were carried out at the light source PETRA III at DESY, a member of the Helmholtz Association (HGF). The XFEL experiments were performed at BL3 of SACLA with the approval of the Japan Synchrotron Radiation Research Institute (JASRI) (proposal nos. 2013A8010 and 2015B8015). **Funding:** This work was supported by the Clusters of Excellence "The Hamburg Centre for Ultrafast Imaging" (EXC 1074, project ID 194651731) and "Advanced Imaging of Matter" (EXC 2056, project ID 390715994) of the Deutsche Forschungsgemeinschaft (DFG).
Author contributions: F.L., B.H., C.G., and G.G. wrote the research proposals. B.H. synthesized and prepared the samples. B.R. and M.S. prepared the experimental setup and supervised the experimental procedures at ESRF and PETRA III, respectively. T.K., K.T., M.Y., and T.I. prepared the experimental setup and supervised the experimental procedures at SACLA. F.L., B.H., L.M., M.A.S., D.S., and G.G. performed the storage-ring experiments; F.L., B.H., M.A.S., C.G., and G.G. performed the experiment at SACLA. F.L. analyzed the data, and F.L. and G.G. interpreted and modeled the data. F.L. wrote the manuscript text, with input from all authors. **Competing interests:** The authors declare that they have no competing interests. **Data and materials availability:** All data needed to evaluate the conclusions in the paper are present in the paper and/or the Supplementary Materials. Additional data related to this paper may be requested from the authors.

Submitted 2 May 2020
Accepted 4 September 2020
Published 21 October 2020
10.1126/sciadv.abc5916

Citation: F. Lehmkühler, B. Hankiewicz, M. A. Schroer, L. Müller, B. Ruta, D. Sheyfer, M. Sprung, K. Tono, T. Katayama, M. Yabashi, T. Ishikawa, C. Gutt, G. Grübel, Slowing down of dynamics and orientational order preceding crystallization in hard-sphere systems. *Sci. Adv.* **6**, eabc5916 (2020).

Slowing down of dynamics and orientational order preceding crystallization in hard-sphere systems

Felix Lehmkühler, Birgit Hankiewicz, Martin A. Schroer, Leonard Müller, Beatrice Ruta, Dina Sheyfer, Michael Sprung, Kensuke Tono, Tetsuo Katayama, Makina Yabashi, Tetsuya Ishikawa, Christian Gutt and Gerhard Grübel

Sci Adv **6** (43), eabc5916.
DOI: 10.1126/sciadv.abc5916